PCCP

Cite this: *Phys. Chem. Chem. Phys.*, 2012, **14**, 16286–16293

www.rsc.org/pccp

PAPER

Controlled evaporative self-assembly of poly(3-hexylthiophene) monitored with confocal polarized Raman spectroscopy

Guihua Xiao,[a] Yan Guo,[a] Yuan Lin,*[a] Xiaojing Ma,[a] Zhaohui Su*[a] and Qian Wang[b]

Received 28th September 2012, Accepted 15th October 2012
DOI: 10.1039/c2cp43435k

Highly-ordered, parallel gradient P3HT stripes are fabricated through a facile deposition method based on controlled evaporative self-assembly (CESA). Confocal polarized Raman spectroscopy is employed to determine the orientation of P3HT chains in individual stripes and spacing. This is the first report on orientation at the molecular level, beyond sole morphology, in the patterns assembled by CESA. P3HT chains tend to aggregate into one-dimensional nanowhiskers in solution upon aging, leading to a time-evolved dispersion composed of isolated chains and nanowhiskers. A corresponding evolution of morphology and molecular orientation in the obtained patterns is observed when assembling P3HT solutions with different aging times. The stripes evolve gradually from slim stripes with fingering instabilities for fresh solution into highly regular, perfect stripes for sufficiently aged solution. In the stripe region, P3HT backbone chains align parallel to the contact line for fresh solution whereas perpendicular for aged solution. The thermodynamic multicomponent system gives greater variety to the CESA study.

1. Introduction

When a spilled drop of coffee dries on a surface, it forms a ring structure along the perimeter, this is the so-called "coffee ring" phenomenon.[1] The contact line can stay pinned to generate a single ring[1] or shrink in a discontinuous manner (*i.e.*, "stick–slip" motion) to form multiple rings.[2] This phenomenon has been widely utilized to fabricate patterned surfaces,[3–5] where precise control over the contact line plays a vital role in producing well-ordered patterns. In recent years, controlled evaporative self-assembly (CESA) in confined geometries has been developed into a facile and robust technique to obtain ordered structures.[6–18] Through subjecting solution to a restricted geometry, the evaporation is constrained to occur at the droplet edge rather than over the entire surface, and thus patterns of high regularity can be produced.[19] This CESA method has vast advantages, such as being nonlithographic, external-field-free, simple and inexpensive.[19] Besides, it is scalable to large areas, and can produce well-organized two dimensional or even three dimensional patterns using less solution.[12,13,19,20] So far, this assembly method has been applied to a wide range of materials, such as inorganic nanoparticles,[9] polymers,[6–8,16,17] and biological entities.[13,21] However, previous studies mainly focused on patterning rather than aligning subjects *via* this technique.[6–8,14–17] Few studies involved anisotropic particles, and their orientation was investigated using microscopic techniques, such as atomic force microscopy (AFM), transmission electron microscopy (TEM), and scanning electron microscopy (SEM).[11–13] Orientation of materials at the molecular scale within the assembled patterns obtained *via* CESA has rarely been studied.

Molecular orientation of materials can be characterized by many techniques such as wide-angle X-ray diffraction (WAXD), birefringence measurements and molecular spectroscopy techniques.[22] Among these techniques, polarized Raman spectroscopy stands out as a powerful tool due to its considerable advantages. It requires little sample preparation; it is fast and non-destructive and suitable for remote analysis; very high spatial resolution can be achieved *via* confocal Raman microscopy.[22,23] Notably, the high spatial resolution enables quantification of molecular orientation and structure even in individual nanofibers.[23–25] Therefore, it should be quite effective for the evaluation of molecular alignment in individual stripes within the patterns produced by CESA.

Poly(3-hexylthiophene) (P3HT) has emerged as a promising candidate for organic field effect transistors and organic solar cells due to its high charge carrier mobility, excellent film-forming properties and fine environmental stability.[26–30] In organic devices, film morphology has been reported to have strong effects on the performance of the devices.[31–34] Orientation of P3HT chains in a thin film is highly desirable because of its strong anisotropy in charge transport, where the charge carrier mobility along the π–π stacking and conjugated backbone

[a] *State Key Laboratory of Polymer Physics and Chemistry, Changchun Institute of Applied Chemistry, Chinese Academy of Sciences, Changchun 130022, PR China. E-mail: linyuan@ciac.jl.cn, zhsu@ciac.jl.cn*
[b] *Department of Chemistry and Biochemistry, University of South Carolina, 631 Sumter Street, Columbia, South Carolina 29208, USA*

chain direction can be several orders of magnitude higher than that along the lamellar stacking direction consisting of insulating side chains.[27,32,35] Nowadays, various methods have been applied to orient P3HT chains in the plane of a substrate.[36–41] However, these methods are either complicated or expensive or with the assistance of external mechanical forces or limited in producing ordered patterns of large-areas.

In our previous study, we have employed capillary tubes,[13] parallel plates[42] and cylinder-on-flat geometry[43] to construct confined space, and highly-ordered, large-scale stripe patterns with aligned rod-like nanoparticles have been obtained. These dispersions are usually in a thermodynamically equilibrium state, whose compositions do not evolve with time. Herein, we studied the CESA of a thermodynamically non-equilibrium dispersion, P3HT solution in chloroform. P3HT chains tend to crystallize and aggregate into one-dimensional nanowhiskers *via* π–π stacking in solution during storage (aging process),[32] leading to a time-evolved system with diverse structures and multiple components at different length scales.[44–46] This dynamic multicomponent dispersion will give greater functionality and variety to the CESA study. An evolution of morphology was observed upon solution aging. Moreover, we further evaluated the orientation of P3HT backbone chains in individual stripes and spacings *via* confocal polarized Raman spectroscopy. To the best of our knowledge, this is the first report on orientation at the molecular level, beyond sole morphology, in CESA patterns. A development in the orientation of P3HT chains in the stripe region and the spacing region within patterns obtained from solutions with different aging times was analyzed *via* confocal polarized Raman spectroscopy.

2. Experimental

2.1 Controlled evaporative self-assembly (CESA) of P3HT chloroform solution

Regioregular P3HT (M_w = 45 000 Da, PDI = 2.0, RR = 98%) was purchased from Rieke Metals Inc. and used without further purification. P3HT was dissolved in chloroform at a concentration of 0.1 mg mL^{-1} at ~60 °C and then aged at room temperature (~14 °C) in tightly closed vials wrapped with aluminum foils. The Si substrates (1.5 cm × 1.5 cm) and cylindrical lenses (L = 12 mm, W = 10 mm, R = 12.92 mm) were cleaned with a piranha solution (7 : 3 98% H_2SO_4–30% H_2O_2) at 80 °C for 2 h to remove stains on the surface (***Caution! Piranha solution reacts violently with organic materials.***), then washed thoroughly with deionized water and dried under nitrogen flow. The cylinder-on-flat geometry was constructed as shown in Fig. 1, with cylindrical lenses situated on a flat substrate. P3HT chloroform solution (30 μL) was trapped within the gap between the cylinder and Si due to the capillary force. After evaporation (less than half an hour), gradient parallel stripes were obtained on the Si substrates. Although the stripe patterns were produced on both the cylinder and Si surfaces, only the patterns formed on Si were evaluated.

2.2 Characterization

Raman spectra were obtained with LabRam HR800 spectrometer (Horiba Jobin Yvon) equipped with an Olympus BX41 microscope in the backscattering geometry. Both the confocal hole and the slit width were fixed at 200 μm. A 632.8 nm He–Ne laser was focused on the sample with a 50× objective lens (0.75 NA). Under this condition, the spatial resolution of the beam spot is around 1 μm. The power at the sample was ~1.8 mW for the stripe while 6.8 mW for the spacing. A half-wave plate was used to select the polarization of the incident laser beam and a polarizer was used to select the polarization of the scattered beam. A scrambler was placed before the 600 grooves per mm holographic grating in order to minimize its polarization-dependent response. Stripes were aligned along the Z direction as shown in Fig. 1d and polarized spectra were recorded in the order: ZZ, XX. For Fig. 6, ratios were obtained by measuring ten different points in one stripe in the outer region (Fig. 1c).

UV–vis absorption spectra were recorded with TU-1901 (Beijing Purkinje General Instrument Co., Ltd.). The optical length of the liquid cell is 2 mm. Optical microscopy measurements were carried out using a Carl Zeiss A1m microscope with a charge-coupled device camera. AFM characterization was obtained on an Agilent 5500 AFM by tapping mode in an ambient atmosphere.

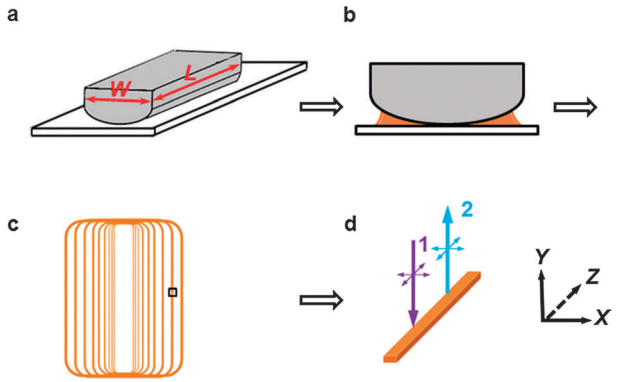

Fig. 1 (a) Cylinder-on-flat evaporation setup. W and L are the width and length of the cylindrical lens, respectively. (b) A drop of P3HT solution (indicated in orange color) placed in a cylinder-on-flat geometry (side view). (c) Representation of gradient stripes formed upon evaporation on Si surface. The square marks the region studied by confocal polarized Raman spectroscopy. (d) An enlarged view of one stripe marked in (c) and the experimental geometry in confocal polarized Raman measurements. X, direction perpendicular to the stripe axis in the sample plane; Y, propagation direction of incident laser light (arrow 1) and of back scattered light (arrow 2); Z, stripe axis.

3. Results and discussion

3.1 Controlled evaporative self-assembly of P3HT chloroform solution

As shown in Fig. 1, P3HT chloroform solution was placed in the cylinder-on-flat geometry to form a capillary-held solution, and the evaporation of chloroform was restricted to occur at the capillary edge. Evaporative loss of chloroform at the edge was replenished by the interior liquid. P3HT was carried to the periphery by the outward flow, and then deposited along the contact line ("stick" process). During the deposition of P3HT, the initial contact angle of the meniscus gradually decreased

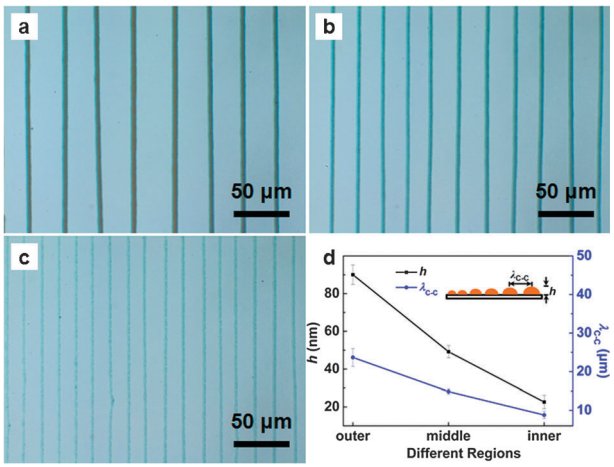

Fig. 2 (a–c) OM images of gradient stripes produced from assembling 0.1 mg mL^{-1} P3HT chloroform solution preserved for 14 days in the (a) outer region, (b) middle region, and (c) inner region, respectively. (d) Values of λ_{C-C} (blue dots) and h (black squares) in different regions. The definition of λ_{C-C} and h is illustrated in the inset.

due to the evaporation of chloroform, to a critical angle, at which the capillary force (depinning force) became stronger than the pinning force.[6] This caused the contact line to jerk towards the contact center ("slip" process) and get arrested at a new position. At this new position, the contact line was pinned again and a new ring could be formed. Highly-ordered and parallel stripes were formed by the consecutive "stick–slip" motion of the receding contact line. Since the "stick–slip" motion of the contact line was governed by the competition between the linear pinning force and the nonlinear depinning force,[6] gradient stripes were finally fabricated. Both the center-to-center distance between adjacent stripes (λ_{C-C}) and the height of the stripe (h) decrease with increasing proximity to the contact center of the cylinder-on-Si geometry (Fig. 2d). Moreover, the width of the stripe as well as the spacing decreases with approaching the contact center, as shown in the optical microscopic (OM) images (Fig. 2a–c). The width of the stripe is 6.3 ± 0.2 μm in the outer region, 4.8 ± 0.2 μm in the middle region and 3.5 ± 0.3 μm in the inner region. The corresponding width of the spacing is 17.6 ± 2.2 μm, 10.1 ± 0.7 μm and 5.4 ± 0.9 μm, respectively.

3.2 Evolution of morphology upon solution aging

Under specific conditions, P3HT chains in solution exhibit a strong tendency towards crystallization and aggregation,[32] resulting in a dispersion with isolated chains, nanowhiskers and their aggregates.[44–48] The aging process of P3HT solution is accompanied by color change,[49,50] which can be monitored by UV–vis spectroscopy.[45–47,51,52] Here, P3HT chloroform solution was stored in dark at room temperature and examined at different aging times. Crystalline aggregates of P3HT molecules form and grow in chloroform solution upon aging,[51] which is reflected in UV–vis spectra (Fig. 3). The freshly prepared solution is orange in appearance, and the absorption spectrum exhibits a broad and featureless absorption with a maximum at 452 nm (Fig. 3), which indicates a coiled conformation of P3HT chains.[45,46,52,53] Upon aging, the color of the solution changes

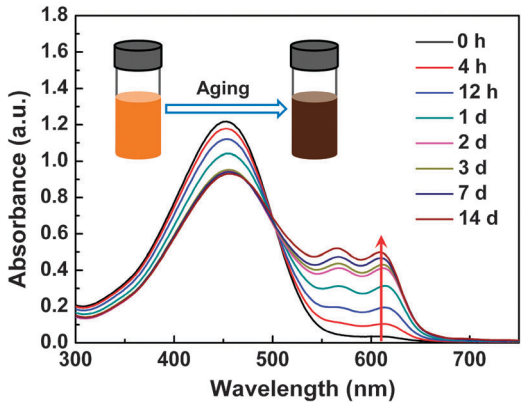

Fig. 3 UV–vis absorption spectra of 0.1 mg mL^{-1} P3HT chloroform solution aged for different times. The red arrow indicates the emergence of the peaks at 610 nm upon aging. The inset shows the solution color at 0 h and 14 days.

from orange to purple and finally to brown (Fig. 3, inset). Meanwhile, additional peaks at lower energy bands (around 565 nm and 610 nm) develop in UV–vis absorption spectra and increase upon solution aging, with the main absorption band decreasing. The absorption peak at 565 nm is attributed to 0–0 transition of the intrachain excitons,[53] whereas the peak at ~610 nm originates from the interchain π–π* transition of P3HT,[45,46,53] which has been used to monitor the crystallization process of P3HT from solution *in situ*.[45–47,51,54,55] The increased absorption intensity at 610 nm means more π–π stacking, which can be due to larger population of crystalline aggregates or longer crystalline aggregates.[45,50–52] So the emergence of the two new peaks as well as the main absorption demonstrates the coexistence of two P3HT phases in the solution during aging: well dissolved P3HT chains and crystalline aggregates.[44,45,48,52] Atomic force microscopy (AFM) and transmission electron microscopy (TEM) techniques can also be used to monitor the formation and growth of the nanowhisker aggregates.[45,51,52] TEM images of P3HT drop cast from its solution aged for different times are shown in Fig. 4a–d, which demonstrate the formation and growth of nanowhiskers in P3HT solution during storage. For the freshly prepared solution, no nanowhisker is observed. Upon aging, nanowhiskers appear, and their average length gradually increases, from ~1.4 μm for 4 h to ~2.6 μm for 12 h. For the solution aged for 5 days, the nanowhiskers are long and form a network so that it is difficult to measure the length of individual nanowhiskers. Fig. 4e illustrates the evolution of P3HT aggregation in chloroform solution during the aging process. Initially, P3HT chains are well dissolved in chloroform. Upon cooling to room temperature, the fresh solution becomes oversaturated and P3HT starts to crystallize slowly, and therefore P3HT isolated chains and nanowhiskers coexist with their ratio changing with aging time.

Stripes parallel to the contact line can be produced from 0.1 mg mL^{-1} P3HT chloroform solution irrespective of the aging time, which is due to the repeated "stick–slip" motion of the contact line discussed above. However, since the coexisting multiple components in P3HT chloroform solution evolve upon aging, the morphology of the assembled patterns obtained is expected to depend on the aging time of the solution as well, as seen in Fig. 5. Stripes fabricated from the as-prepared solution

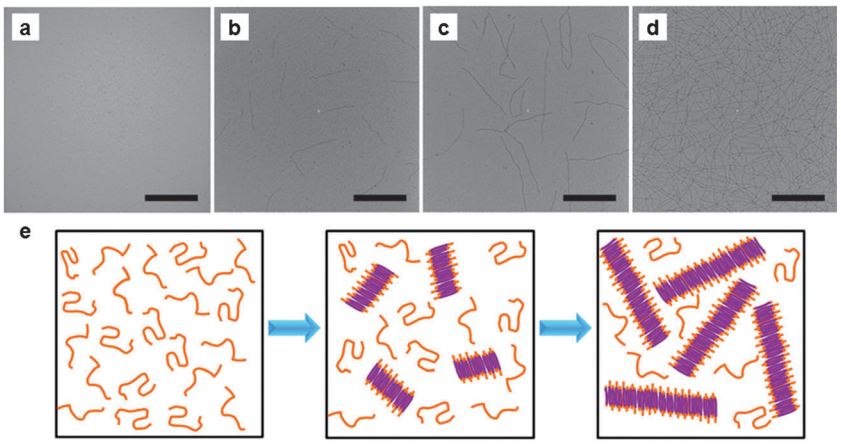

Fig. 4 TEM images of P3HT nanowhiskers from chloroform solution (0.1 mg mL^{-1}) aged for different times: (a) 0 h, (b) 4 h, (c) 12 h, and (d) 5 days. Scale bars represent 2 μm. (e) Schematic illustration of the formation and growth of P3HT nanowhiskers in solution upon aging. The coils in orange indicate well-dissolved chains, and the rod-like structures in purple represent nanowhiskers.

are not uniform, representing as slim stripes with many fingering instabilities (Fig. 5a and d).[7,8] The fingering instabilities are manifested as surface perturbations with a well-defined wavelength at the edges of a ring.[7] The slim parts are so thin that they are barely visible in the OM images (Fig. 5a); the continuity of the stripes is confirmed by AFM (Fig. 5d). However, the perturbations are vanishing upon solution aging while the slim straight parts mount up, and eventually highly-ordered, uniform stripes are obtained (Fig. 5b,c and g). The detailed microstructures in the stripe region and spacing region of the patterns produced from solutions with different aging times can be easily detected from the enlarged AFM images (Fig. 5e,f,h and i). Notably, the surface features of the spacing differ significantly. When the solution is fresh, there are a few dot-like structures left on the spacing after evaporation, while densely packed nanowhiskers taking an orientation perpendicular to the contact line are produced in the spacing for the solution aged for 7 days (Fig. 5f and i).

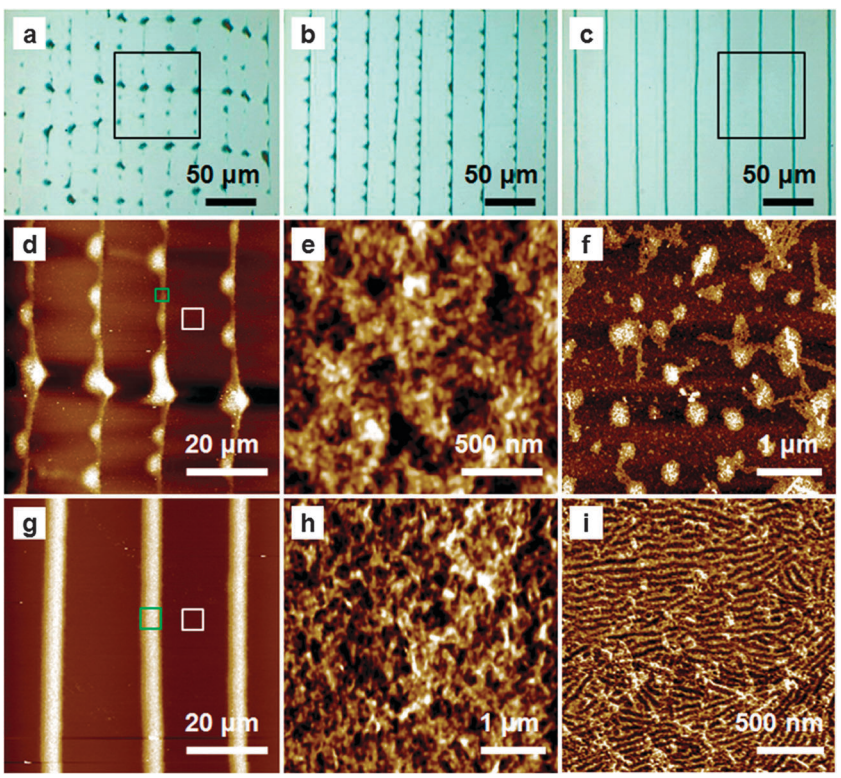

Fig. 5 Stripe patterns formed in the outer region from P3HT chloroform solution (0.1 mg mL^{-1}) aged for different times. (a–c) OM images of P3HT stripe patterns formed from solutions aged for (a) 0 h, (b) 12 h, and (c) 7 days, respectively. Darker regions are the stripes. (d–i) AFM topography images of P3HT patterns. (d) An enlarged view of the square in (a). (e, f) Enlarged views of the (e) green and (f) white square regions in (d), respectively. (g) An enlarged view of the square in (c). (h, i) Enlarged views of the (h) green and (i) white square regions in (g), respectively.

The evolution of morphology upon solution aging can be explained as follows. As the chloroform evaporates, P3HT is transported to the capillary edge by capillary flow[1] and deposited at the contact line, where one stripe is formed. When the solution is fresh, P3HT is finely dissolved and adopts a coiled conformation,[44–47,51,52] with smaller nonvolatile solute[44–47] and lower viscosity.[54,56] As a result, the pining force is not strong and fingering defects at a propagating front may develop.[7,8] To a certain extent, the pattern fabricated from the fresh solution resembles the "snake-skin" structures obtained by Lin and coworkers.[8] Dot-like structures left on the spacing after evaporation may be attributed to dewetting of the solution caused by solvent evaporation.[47,52,57] When the solution is sufficiently aged, significant amounts of nanowhiskers are present whose dimensions are larger than P3HT coiled chains and the solution is stickier.[44–47,54,56] This leads to a larger pinning force, resulting in regular stripes without fingering instabilities.[7] The fact that the nanowhiskers are deposited easier than coiled chains is also evidenced from enlarged views of the spacing (Fig. 5f and i). Much more deposition composed of aligned nanowhiskers is observed for aged solution. The orientation of the nanowhiskers in the spacing can be attributed to the shearing force exerted by the "skip" motion of the contact line, which is rather quick when taking the evaporation rate of chloroform into consideration.

3.3 Evolution of molecular orientation upon solution aging

The dynamic multiple components in solution lead to an evolution of the morphology within P3HT patterns. However, the morphological images provide no information on the molecular orientation of P3HT backbones within the assembled patterns. Here we use confocal polarized Raman spectroscopy to characterize the orientation of P3HT chains in individual stripe and spacing. Polarized Raman spectroscopy is a robust technique to quantify molecular orientation and has been applied in the study of P3HT in several reports.[58,59] Fig. 1d shows the experimental geometry of the polarized Raman measurements. We define Z direction as that parallel to the long axis of the stripe and X perpendicular to the stripe long axis in the sample plane. For the measurements with polarized light, we use two configurations, ZZ and XX, using the notation "incident polarization analyzed polarization" as described in literatures.[22–24] More specifically, the first letter corresponds to the polarization of the incident beam and the second to the selected component of the scattered beam. We chose the outer region (Fig. 1c) for orientation study to make sure that there is a similar thermal history to the bulk solution. The spatial resolution of the confocal Raman microscope used in this study is around 1 μm, sufficient to assess the molecular orientation within individual stripes and spacing, the minimum width of which is 1.5 and 10 μm, respectively. Fig. 6a shows two sets of polarized Raman spectra in the 610–1750 cm^{-1} region of one stripe within P3HT patterns formed from solutions aged for 0 h and 3 days, respectively. Here we mainly focus on the in-plane ring skeleton modes at $\sim$1445 cm^{-1} (symmetric $C_\alpha{=}C_\beta$ stretching vibrations),[60] as marked in the red rectangle in Fig. 6a. We employ the Raman anisotropy, $R = I_{ZZ}/I_{XX}$, to characterize the molecular orientation, where I_{ZZ} and I_{XX} are the Raman scattering intensities in the ZZ and XX configuration, respectively. For random (isotropic) orientation, $R = 1$, whereas for the perfect uniaxial alignment $R = \infty$.[61] In our experiment, the R value is 1.1 ± 0.1 for the spin-coated film, which indicates no preferred orientation. For the stripes assembled from fresh solution, I_{ZZ} is much larger than I_{XX}, which indicates an anisotropic ordering of P3HT rings and more P3HT backbone chains are aligned along the Z direction, *i.e.* parallel to the stripes (Fig. 1d). Since for the freshly prepared P3HT solution the dominant assembly objects are finely dissolved P3HT chains, a much larger I_{ZZ} means more P3HT chains are oriented parallel to the contact line. However, for patterns assembled from the solution aged for 3 days, a much smaller I_{ZZ} than I_{XX} is obtained, indicating perpendicular orientation of P3HT chains in the stripes. As discussed in previous sections, in the sufficiently aged solution more nanowhiskers form, in which P3HT backbones are perpendicular to the long axis of the nanowhiskers.[32,49] Therefore the Raman data suggest that the nanowhiskers deposited preferentially orient parallel to the contact line in stripes.

The evolution in Raman anisotropy of the 1445 cm^{-1} peak could be used to monitor the temporal development of molecular orientation upon solution aging. Raman anisotropy in both the stripe region and the spacing region was recorded (Fig. 6b and c). Raman anisotropy of the stripe decreases from $\sim$1.7 for fresh solution, to $\sim$1.0 (solution aged for 12 h) and finally to $\sim$0.4 (solution aged for 3 days or longer). In the spacing region, on the other hand, the Raman anisotropy value is $\sim$1.1 for the as-prepared solution, and it gradually increases to $\sim$2.0 (solution aged for 3 days) and plateaus for longer aging times. As mentioned above, individual coiled chains are the majority in the fresh solution and they are difficult to settle due to the smaller size[44–47] and lower viscosity[54,56] in solution. Even if some are deposited, dot-like structures with no preferred orientation are formed, which is possibly due to the dewetting of chloroform solution.[47,52] However, in aged solution, more nanowhiskers form, which favor deposition due to larger dispersate size[44–47] and increased solution viscosity.[54,56] These nanowhiskers tend to align perpendicular to the contact line in the spacing under shear, *i.e.*, the P3HT chains are parallel to the contact line in the spacing, resulting in a much higher I_{ZZ} than I_{XX}.

For the patterns obtained from sufficiently aged solution (3 days or longer), the Raman anisotropy value is $\sim$0.4 in the stripe region and $\sim$2 in the spacing region. This indicates that P3HT chains align perpendicular to the contact line in the stripe region while parallel in the spacing region. A similar structure has been reported by Lee and co-workers in the assembly of rod-like bacteriophage M13.[62]

3.4 Mechanism analysis for the evolution of morphology and orientation upon solution aging

Experimental observations in previous sections have provided significant insight into the mechanism of different assembly behaviors of P3HT solutions with different aging times. P3HT chains tend to aggregate into one-dimensional nanowhiskers in solution, so the P3HT solution is thermodynamically unstable. It is a multicomponent dispersion composed of isolated chains

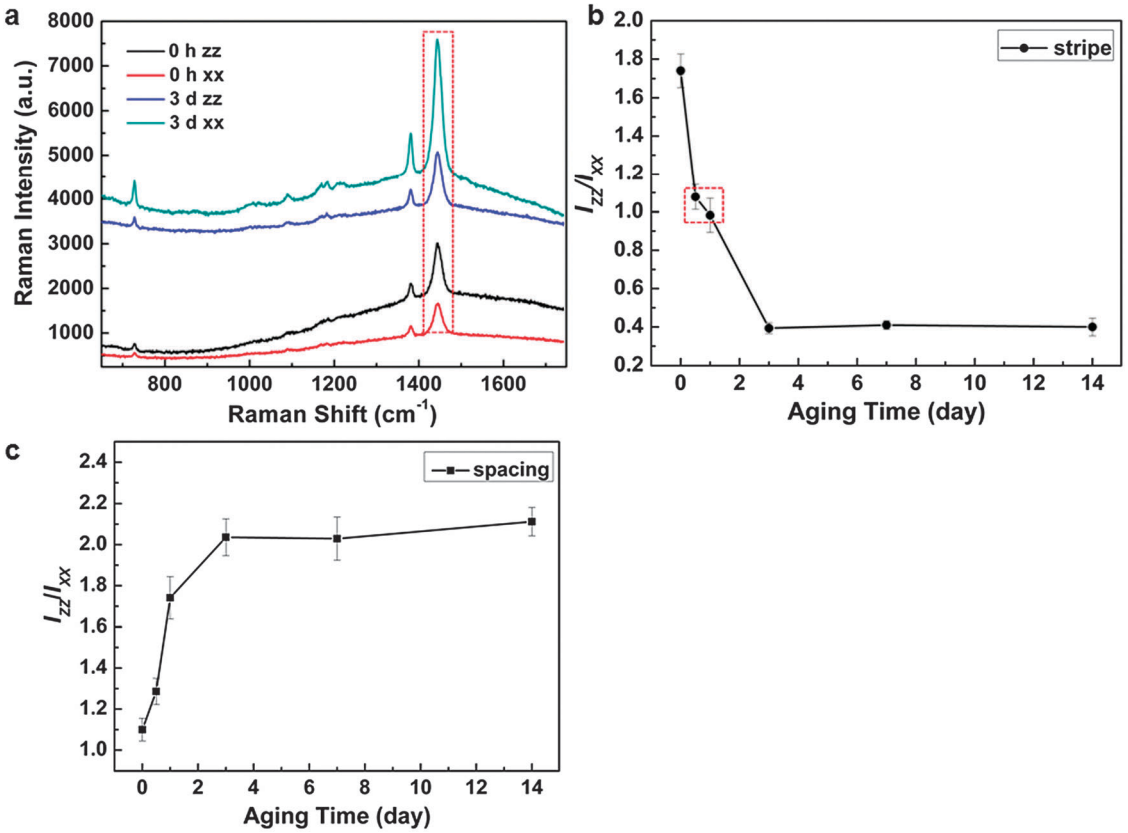

Fig. 6 (a) Polarized Raman spectra of P3HT stripes formed from solutions aged for 0 h and 3 days, respectively (0.1 mg mL^{-1} P3HT in chloroform). Red rectangle highlights the band of interest. (b) and (c) Raman anisotropy (I_{ZZ}/I_{XX}) of the 1445 cm^{-1} peak for the stripe region (b) and spacing region (c) formed from 0.1 mg mL^{-1} P3HT chloroform solution with different aging times. The red rectangle highlights the transition region of the molecular orientation.

and nanowhiskers, evolving with time. In fresh solution there are only coiled chains. When the evaporation happens, these chains are driven to the edge of the contact line. Anisotropic string-like objects tend to orient parallel to the plane of the interface in order to maximize the interfacial coverage per particle (Fig. 7b).[63] After evaporation, stripes with parallel aligned P3HT chains to the contact line are fabricated. Since the dissolved coiled chains are difficult to deposit due to the smaller size of the assembly entity and lower viscosity of the solution,[44–47,54,56] the pinning force is weaker and fingering instabilities develop (Fig. 5a and d).[7,8] Only a few dot-like structures are obtained in the spacing (Fig. 5f)

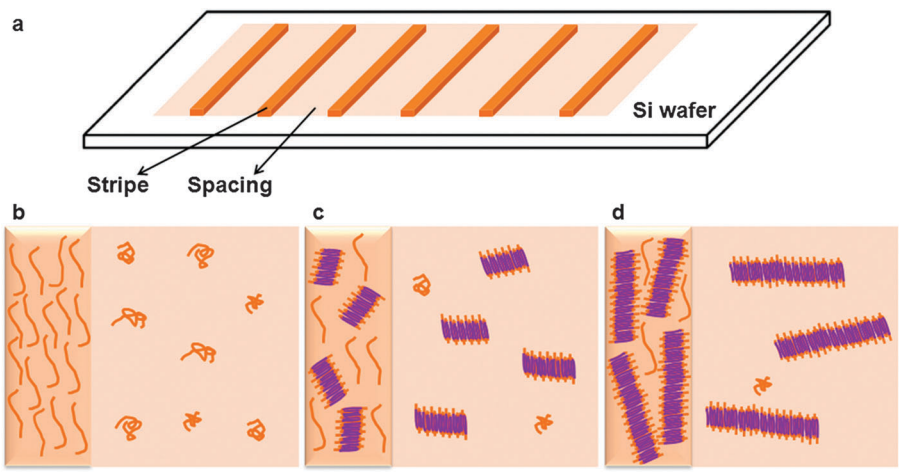

Fig. 7 Schematic illustration of the evolution of stripes and spacings with increasing aging time. (a) P3HT stripe pattern formed on Si wafer after evaporation. (b–d) Microstructure of stripe and spacing obtained from solutions with increasing aging time. The coils in orange indicate well-dissolved chains, while the rod-like structures in purple represent nanowhiskers.

and no favored orientation is observed by polarized Raman spectroscopy (Fig. 6).

Upon aging, more and more nanowhiskers appear while the amount of coiled chains decreases. At the three phase contact line, the anisotropic nanowhiskers tend to orient parallel to the contact line upon evaporation to maximize the interfacial coverage per particle[63] (Fig. 7c and d). Within the stripes, although nanowhiskers align parallel to the contact line, P3HT chains in the nanowhiskers are indeed perpendicular to the contact line. Thus the time-evolved coexisting coiled chains and nanowhiskers compete in molecular orientation. In other words, if individual chains dominate in the solution, the overall orientation of P3HT chains is parallel to the contact line; whereas for nanowhiskers, the overall orientation of P3HT chains is perpendicular. The conversion of individual molecules into nanowhiskers leads to the decrease in I_{ZZ}/I_{XX} with increased aging time of the solution. When these two kinds of orientation cancel each other out, Raman anisotropy of $\sim$1 is detected (Fig. 6b, highlighted in red rectangle) and a transition region appears. With larger assembly entities and increased viscosity,[44–47,54,56] the pinning force is strong enough to achieve highly regular stripes and suppress fingering instabilities (Fig. 5b,c and g).[7,8] As for the spacing, easily deposited nanowhiskers are aligned perpendicular to the contact line under shearing forces during the "slip" process due to their anisotropic shape (Fig. 5i,7c and d) and a Raman anisotropy value greater than 1 is obtained.

Therefore, the time-evolved coexisting multiple components in the solution result in the development of morphology and molecular orientation within the assembled patterns upon solution aging. Parallel, straight and highly ordered P3HT stripes can be produced through this one-step assembly process using a sufficiently aged P3HT solution. Remarkably, a very interesting structure with parallel alignment of nanowhiskers to the contact line in the stripe region but perpendicular alignment of nanowhiskers in the spacing region has been obtained (Fig. 7d), which may have potential applications in organic field effect transistors and organic solar cells.

4. Conclusions

We have assembled P3HT chloroform solutions with different aging times through CESA. Both OM and AFM results showed an evolution of morphology upon solution aging. The stripes transformed from slim stripes with fingering instabilities for fresh solution into uniform, straight, highly regular stripes for aged solution. A development in molecular orientation was also observed due to solution aging. A right angle rotation of P3HT chain orientation can be achieved just by assembling P3HT solutions with different aging times. Molecular orientation of P3HT in the spacing region was also investigated. An interesting structure with nanowhiskers parallel aligned in the stripe region but perpendicular aligned in the spacing region can be achieved, which may have unique optical, electronic or photonic properties. Engineering this self-assembly method may offer potential applications in P3HT-based organic devices.

Acknowledgements

This work is supported by the National Natural Science Foundation of China (21128002, 21104080, and 20990233). Z.S. acknowledges the NSFC Fund for Creative Research Groups (50921062) for support.

References

1 R. D. Deegan, O. Bakajin, T. F. Dupont, G. Huber, S. R. Nagel and T. A. Witten, *Nature*, 1997, **389**, 827–829.
2 L. Shmuylovich, A. Q. Shen and H. A. Stone, *Langmuir*, 2002, **18**, 3441–3445.
3 J. X. Huang, F. Kim, A. R. Tao, S. Connor and P. D. Yang, *Nat. Mater.*, 2005, **4**, 896–900.
4 C. Y. Zhang, X. J. Zhang, X. H. Zhang, X. Fan, J. S. Jie, J. C. Chang, C. S. Lee, W. J. Zhang and S. T. Lee, *Adv. Mater.*, 2008, **20**, 1716–1720.
5 H. Y. Li, B. C. K. Tee, J. J. Cha, Y. Cui, J. W. Chung, S. Y. Lee and Z. N. Bao, *J. Am. Chem. Soc.*, 2012, **134**, 2760–2765.
6 J. Xu, J. F. Xia, S. W. Hong, Z. Q. Lin, F. Qiu and Y. L. Yang, *Phys. Rev. Lett.*, 2006, **96**, 066104.
7 S. W. Hong, J. F. Xia, M. Byun, Q. Z. Zou and Z. Q. Lin, *Macromolecules*, 2007, **40**, 2831–2836.
8 M. Byun, R. L. Laskowski, M. He, F. Qiu, M. Jeffries-El and Z. Q. Lin, *Soft Matter*, 2009, **5**, 1583–1586.
9 H. S. Kim, C. H. Lee, P. K. Sudeep, T. Emrick and A. J. Crosby, *Adv. Mater.*, 2010, **22**, 4600–4604.
10 D. M. Kuncicky, R. R. Naik and O. D. Velev, *Small*, 2006, **2**, 1462–1466.
11 M. Engel, J. P. Small, M. Steiner, M. Freitag, A. A. Green, M. C. Hersam and P. Avouris, *ACS Nano*, 2008, **2**, 2445–2452.
12 Z. L. Wang, R. R. Bao, X. J. Zhang, X. M. Ou, C. S. Lee, J. C. Chang and X. H. Zhang, *Angew. Chem., Int. Ed.*, 2011, **50**, 2811–2815.
13 Y. Lin, E. Balizan, L. A. Lee, Z. W. Niu and Q. Wang, *Angew. Chem., Int. Ed.*, 2010, **49**, 868–872.
14 T. Y. Kim, S. W. Kwon, S. J. Park, D. H. Yoon, K. S. Suh and W. S. Yang, *Adv. Mater.*, 2011, **23**, 2734–2738.
15 S. W. Hong, W. Jeong, H. Ko, M. R. Kessler, V. V. Tsukruk and Z. Q. Lin, *Adv. Funct. Mater.*, 2008, **18**, 2114–2122.
16 W. Han, M. Byun, L. Zhao, J. Rzayev and Z. Q. Lin, *J. Mater. Chem.*, 2011, **21**, 14248–14253.
17 S. W. Kwon, M. Byun, D. H. Yoon, J. H. Park, W. K. Kim, Z. Q. Lin and W. S. Yang, *J. Mater. Chem.*, 2011, **21**, 5230–5233.
18 M. Abkarian, J. Nunes and H. A. Stone, *J. Am. Chem. Soc.*, 2004, **126**, 5978–5979.
19 W. Han and Z. Q. Lin, *Angew. Chem., Int. Ed.*, 2012, **51**, 1534–1546.
20 O. D. Velev and S. Gupta, *Adv. Mater.*, 2009, **21**, 1897–1905.
21 Y. Lin, Z. H. Su, E. Balizan, Z. W. Niu and Q. Wang, *Langmuir*, 2010, **26**, 12803–12809.
22 M. Tanaka and R. J. Young, *J. Mater. Sci.*, 2006, **41**, 963–991.
23 M. Richard-Lacroix and C. Pellerin, *Macromolecules*, 2012, **45**, 1946–1953.
24 S. Pagliara, M. S. Vitiello, A. Camposeo, A. Polini, R. Cingoani, G. Scamarcio and D. Pisignano, *J. Phys. Chem. C*, 2011, **115**, 20399–20405.
25 P. J. Pauzauskie, D. Talaga, K. Seo, P. D. Yang and F. Lagugne-Labarthet, *J. Am. Chem. Soc.*, 2005, **127**, 17146–17147.
26 M. Brinkmann, *J. Polym. Sci., Part B:Polym. Phys.*, 2011, **49**, 1218–1233.
27 H. Sirringhaus, P. J. Brown, R. H. Friend, M. M. Nielsen, K. Bechgaard, B. M. W. Langeveld-Voss, A. J. H. Spiering, R. A. J. Janssen, E. W. Meijer, P. Herwig and D. M. de Leeuw, *Nature*, 1999, **401**, 685–688.
28 K. Y. Jen, G. G. Miller and R. L. Elsenbaumer, *J. Chem. Soc., Chem. Commun.*, 1986, 1346–1347.
29 R. L. Elsenbaumer, K. Y. Jen and R. Oboodi, *Synth. Met.*, 1986, **15**, 169–174.
30 Z. Bao, A. Dodabalapur and A. J. Lovinger, *Appl. Phys. Lett.*, 1996, **69**, 4108–4110.
31 T. L. Benanti and D. Venkataraman, *Photosynth. Res.*, 2006, **87**, 73–81.
32 A. Salleo, *Mater. Today*, 2007, **10**, 38–45.
33 H. C. Yang, T. J. Shin, L. Yang, K. Cho, C. Y. Ryu and Z. N. Bao, *Adv. Funct. Mater.*, 2005, **15**, 671–676.

34 W. Chen, M. P. Nikiforov and S. B. Darling, *Energy Environ. Sci.*, 2012, **5**, 8045–8074.
35 H. Sirringhaus, R. J. Wilson, R. H. Friend, M. Inbasekaran, W. Wu, E. P. Woo, M. Grell and D. D. C. Bradley, *Appl. Phys. Lett.*, 2000, **77**, 406–408.
36 M. Brinkmann and J. C. Wittmann, *Adv. Mater.*, 2006, **18**, 860–863.
37 M. Aryal, K. Trivedi and W. C. Hu, *ACS Nano*, 2009, **3**, 3085–3090.
38 S. Nagamatsu, W. Takashima, K. Kaneto, Y. Yoshida, N. Tanigaki and K. Yase, *Macromolecules*, 2003, **36**, 5252–5257.
39 L. Hartmann, K. Tremel, S. Uttiya, E. Crossland, S. Ludwigs, N. Kayunkid, C. Vergnat and M. Brinkmann, *Adv. Funct. Mater.*, 2011, **21**, 4047–4057.
40 S. Lee, G. D. Moon and U. Jeong, *J. Mater. Chem.*, 2009, **19**, 743–748.
41 B. O'Connor, R. J. Kline, B. R. Conrad, L. J. Richter, D. Gundlach, M. F. Toney and D. M. DeLongchamp, *Adv. Funct. Mater.*, 2011, **21**, 3697–3705.
42 Y. Lin, Z. H. Su, G. H. Xiao, E. Balizan, G. Kaur, Z. W. Niu and Q. Wang, *Langmuir*, 2011, **27**, 1398–1402.
43 G. Xiao, B. Peng, Q. Wang, Z. Su and Y. Lin, *Chin. J. Appl. Chem.*, 2011, **28**, 901–906.
44 G. M. Newbloom, K. M. Weigandt and D. C. Pozzo, *Macromolecules*, 2012, **45**, 3452–3462.
45 W. T. Xu, L. G. Li, H. W. Tang, H. Li, X. L. Zhao and X. N. Yang, *J. Phys. Chem. B*, 2011, **115**, 6412–6420.
46 C. Y. Chen, S. H. Chan, J. Y. Li, K. H. Wu, H. L. Chen, J. H. Chen, W. Y. Huang and S. A. Chen, *Macromolecules*, 2010, **43**, 7305–7311.
47 L. J. Xue, X. H. Yu and Y. C. Han, *Colloids Surf., A*, 2011, **380**, 334–340.
48 S. Berson, R. De Bettignies, S. Bailly and S. Guillerez, *Adv. Funct. Mater.*, 2007, **17**, 1377–1384.
49 S. Samitsu, T. Shimomura, S. Heike, T. Hashizume and K. Ito, *Macromolecules*, 2008, **41**, 8000–8010.
50 M. Koppe, C. J. Brabec, S. Heiml, A. Schausberger, W. Duffy, M. Heeney and I. McCulloch, *Macromolecules*, 2009, **42**, 4661–4666.
51 U. Bielecka, P. Lutsyk, K. Janus, J. Sworakowski and W. Bartkowiak, *Org. Electron.*, 2011, **12**, 1768–1776.
52 L. J. Xue, X. Gao, K. Zhao, J. G. Liu, X. H. Yu and Y. C. Han, *Nanotechnology*, 2010, **21**, 145303.
53 P. J. Brown, D. S. Thomas, A. Kohler, J. S. Wilson, J. S. Kim, C. M. Ramsdale, H. Sirringhaus and R. H. Friend, *Phys. Rev. B: Condens. Matter Mater. Phys.*, 2003, **67**, 064203.
54 W. T. Xu, H. W. Tang, H. Y. Lv, J. Li, X. L. Zhao, H. Li, N. Wang and X. N. Yang, *Soft Matter*, 2012, **8**, 726–733.
55 M. He, L. Zhao, J. Wang, W. Han, Y. L. Yang, F. Qiu and Z. Q. Lin, *ACS Nano*, 2010, **4**, 3241–3247.
56 M. J. Sobkowicz, R. L. Jones, R. J. Kline and D. M. DeLongchamp, *Macromolecules*, 2012, **45**, 1046–1055.
57 M. Ramanathan and S. B. Darling, *Prog. Polym. Sci.*, 2011, **36**, 793–812.
58 M. S. Park, A. Aiyar, J. O. Park, E. Reichmanis and M. Srinivasarao, *J. Am. Chem. Soc.*, 2011, **133**, 7244–7247.
59 H. L. Cheng, J. W. Lin, M. F. Jang, F. C. Wu, W. Y. Chou, M. H. Chang and C. H. Chao, *Macromolecules*, 2009, **42**, 8251–8259.
60 M. Baibarac, M. Lapkowski, A. Pron, S. Lefrant and I. Baltog, *J. Raman Spectrosc.*, 1998, **29**, 825–832.
61 H. M. Liem, P. Etchegoin, K. S. Whitehead and D. D. C. Bradley, *Adv. Funct. Mater.*, 2003, **13**, 66–72.
62 W. J. Chung, J. W. Oh, K. Kwak, B. Y. Lee, J. Meyer, E. Wang, A. Hexemer and S. W. Lee, *Nature*, 2011, **478**, 364–368.
63 J. B. He, Z. W. Niu, R. Tangirala, J. Y. Wan, X. Y. Wei, G. Kaur, Q. Wang, G. Jutz, A. Boker, B. Lee, S. V. Pingali, P. Thiyagarajan, T. Emrick and T. P. Russell, *Langmuir*, 2009, **25**, 4979–4987.